Advances in Science and Technology Research Journal

Volume 13, Issue 2, June 2019, pages 84–91
https://doi.org/10.12913/22998624/106241

Received: 2019.03.05
Revised: 2019.03.21
Accepted: 2019.04.09
Available online: 2019.05.01

# Fatigue Strength of Thin-Walled Rectangular Elements in the State of Post-Critical Deformation

Przemysław Mazurek[1]

[1] Rzeszów University of Technology, The Faculty of Mechanical Engineering and Aeronautics, Al. Powstańców Warszawy 8, 35-959 Rzeszów, Poland, e-mail: pmazurek@prz.edu.pl

**ABSTRACT**

The paper presents the results of numerical analyses and static experimental testing of thin-walled rectangular elements subject to post-critical deformation under shear conditions. The deliberations concerned the elements made of aluminium alloy and the model material. The obtained stress distribution was used to conduct a numerical simulation of the fatigue strength for a metal plate and testing under cyclic load conditions for both types of models.

**Keywords:** numerical analysis, fatigue tests, buckling, postbuckling.

## INTRODUCTION

The loss of stability of thin-walled covers occurring under operating load conditions is a commonly encountered phenomenon in contemporary semi-monocoque aviation structures. The occurrence of post-critical deformation is acceptable when the situation concerns the covering segment restricted by rigid structural elements and it has an elastic character. Therefore, the designing process must feature a series of analyses allowing for determining the stress distribution in this type of cases [4, 5]. The fast development of numerical calculation programs based mainly on the finite elements method currently allows for conducting non-linear simulations enabling to determine the state of deformation and stress distribution in any structures [6, 11]. On the basis of the results obtained numerically, it is also possible to designate the fatigue strength of the analysed structures. Obtaining reliable results is especially important due to the cyclic nature of the loads acting on the aviation bearing structures [12, 14]. The large number of factors affecting the initiation of fatigue damage compels constructors to verify the results of numerical calculations experimentally. The appearance of polymer model materials, such as polycarbonate, allows for conducting relatively cheap experimental testing concerning the selected structure fragments.

The results presented in this study constitute a fragment of a broad research program, aimed at elaborating a thin-walled structure designing methodology based on non-linear numerical analyses, verified through experiments conducting using model and real materials.

## SUBJECT AND SCOPE OF RESEARCH

The subject of the testing included flat, thin-walled rectangular structures working under pure shear conditions, imitating a fragment of a semi-monocoque structure covering, placed between rigid framework elements (Fig. 1).

Two types of models were used during testing. The first of them was made of 2024 aluminium alloy with the following parameters: $E = 74000$ MPa, $\nu = 0.33$, $R_{02} = 372$ MPa, $R_m = 470$ MPa, constituting the material commonly employed in aviation. The second element was made using polycarbonate with the trade name "macrolon" and the following parameters: $E = 3000$ MPa, $\nu = 0.36$, $R_c = 50$ MPa, used as the model material. In both cases, the thickness of elements amounted to 0.7 mm.

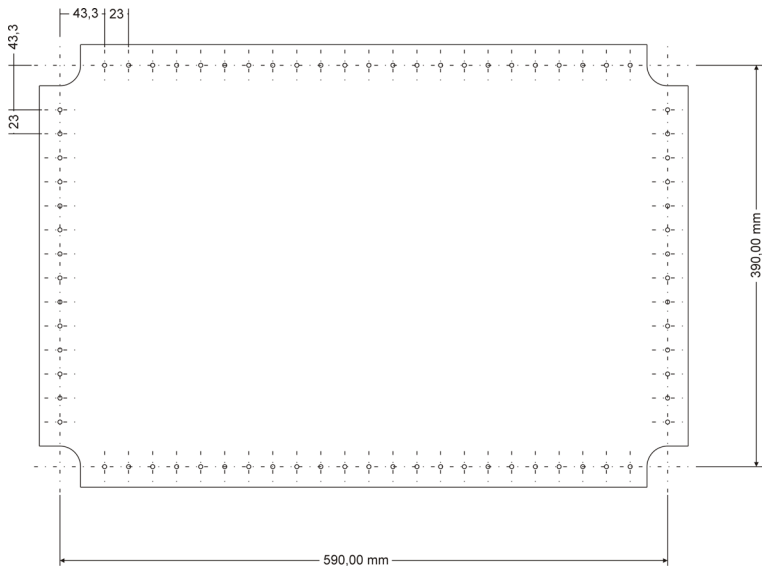


**Fig. 1.** Geometry of the tested objects

The testing was conducted in several stages: static experimental testing allowing for the determination of the form and quantity of the post-critical deformation, non-linear numerical analyses obtaining the stress distribution and predicting the fatigue strength, as well as experimental fatigue testing aimed at ultimate verification of the obtained results. The purpose of the conducted testing was to determine the ability to use the model materials in the preliminary designing stage [13] and conducting comparative tests under cyclic load conditions.

## STATIC EXPERIMENTAL TESTING

The experimental testing was conducted using an installation built into the strength testing cage intended for testing aviation structures. This solution guaranteed a large reserve of system rigidity, which directly contributed to the accuracy of the measurements. The tested structures were mounted in a rigid steel framework, the corners of which were connected with joints. The top right corner was installed in a fixed support with a joint, the top left corner was mounted in a sliding support, whereas the load was applied to the bottom right corner by means of a second-class lever system (Fig. 2). The drive consisted of the Zwick-Roell's electromechanical actuator allowing for applying both static and dynamic loads in cycles programmed according to any load spectrum. The measurements of the reference point displacements and normal deformation distribution in relation to the plate surfaces were conducted using the 3D Atos scanner from GOM.

During the testing, the aluminium alloy element was subjected to force P = 7500N, whereas the polycarbonate element was subjected to force P = 1008 N. The selection of proportions between the forces was dictated in both cases by the ratio of the yield strengths of the materials used.

The conducted testing provided an image of the post-critical deformations for the polycarbonate and aluminium alloy elements. Figure 3 presents the displacement distribution in the form of contour lines obtained as result of 3D scanning.

Special attention should be paid to the difference in the form of deformation between the elements that are identical in terms of geometry. In the case of the polycarbonate plate, dominant, adjacent ridges were formed. The deformation became antisymmetric; the displacements have a similar value and opposite symbols. In the case of the duralumin element, there is a single ridge running along the diagonal, the value of which is substantial higher than the size of other ridges.

## NON-LINEAR NUMERICAL ANALYSIS

The numerical models were generated using the MSC Patran software based on the finite elements method. Figure 4 presents the numerical model including the boundary conditions and the model loading for the aluminium-alloy element. Identical boundary conditions were used in the case of the model material, whereas the load

a)

b)

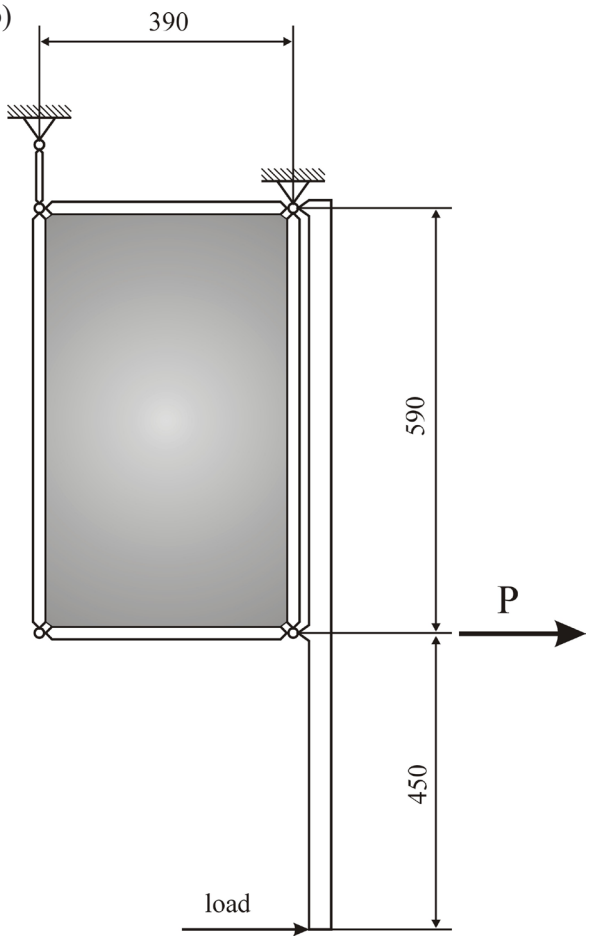


**Fig. 2.** a) measurement station with the 3D Atos scanner, b) loading system diagram

a)

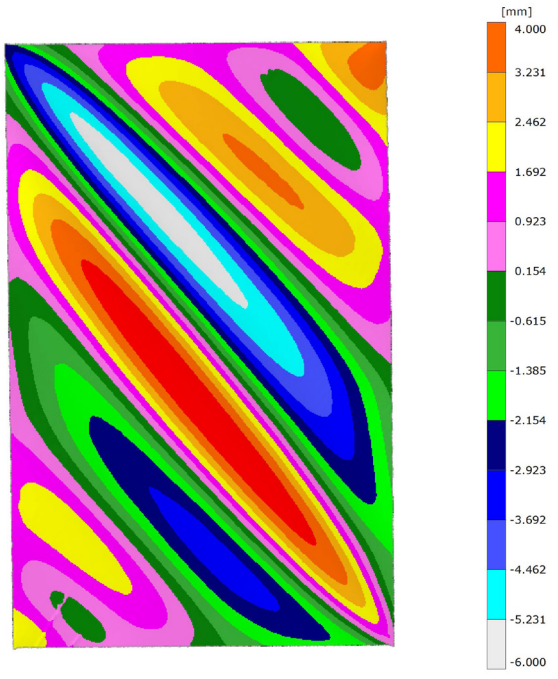


b)

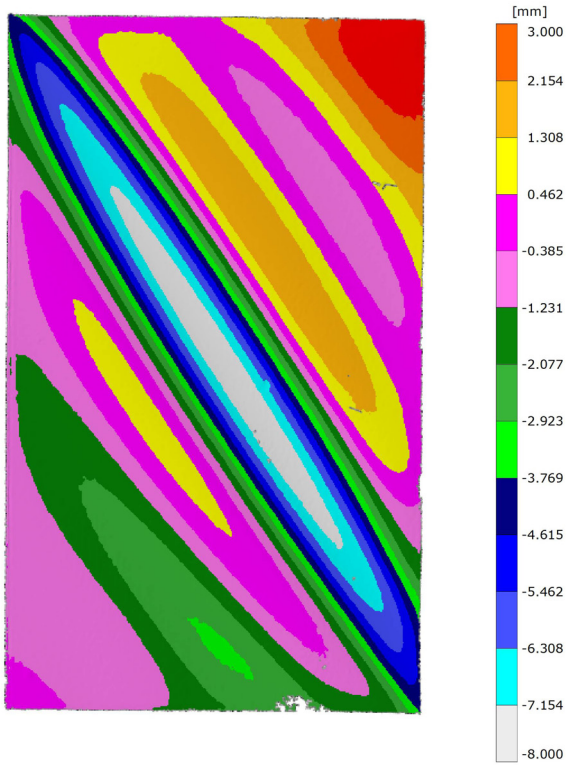


**Fig. 3.** Displacement values obtained as result of scanning: a) polycarbonate element, b) duralumin element

was adapted to the polycarbonate properties and amounted to 1,008 N.

The analysed models consisted of approx. 7,500 thin, shell-type, thin-walled finite elements, whereas the rigid framework was modelled using 3,000 thick, shell-type, finite elements [16]. Continuous connections were used between the rigid mounting framework and the model, in the areas corresponding to the location of bolt connections in a real structure. This was aimed at imitating discrete connections causing local stress concentrations, but also allowed for obtaining a relatively small task size. Usually, such situations include the use of the MPC-type elements [16] allowing for the modelling of discrete connections, but in the case of non-linear procedures they generate numerous errors causing the distortion of results or prevent the solution of a problem. The calculations were conducted using the MSC.Marc solver and applying the Newton-Raphson method, with an adaptive state control [1, 3, 7, 8].

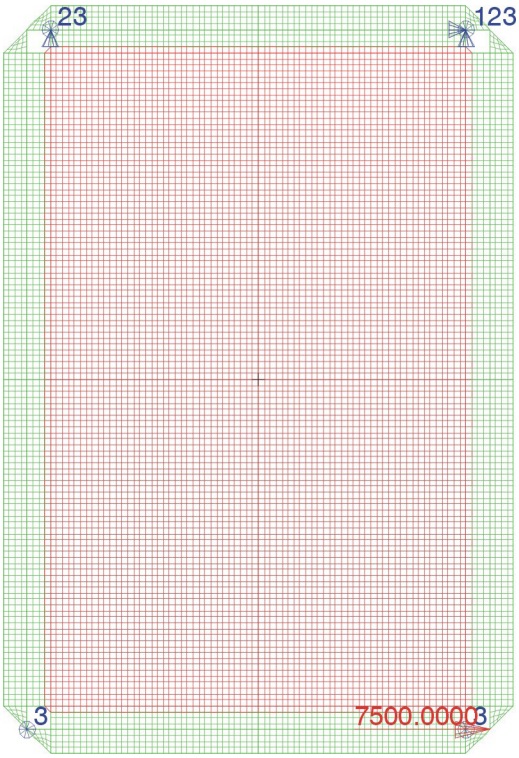


**Fig. 4.** Numerical model of the tested structures

The conducted numerical analyses allowed for obtaining the post-critical deformations fields for both cases of the analysed elements, demonstrating compliance with the values obtained during the 3D scanning, constituting part of the experimental testing. Similarly as in the case of real structures, the polycarbonate plate demonstrated the formation of two dominant, adjacent ridges with opposite displacement signs in the normal direction, in relation to the structure's plane, whereas the duralumin plate is characterised by a single ridge running along the diagonal (Fig. 5).

The presented results of numerical calculations demonstrate high conformity with the

a)

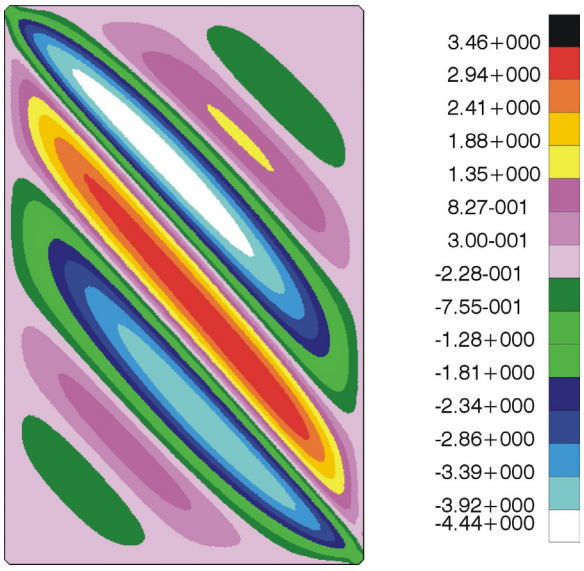


b)

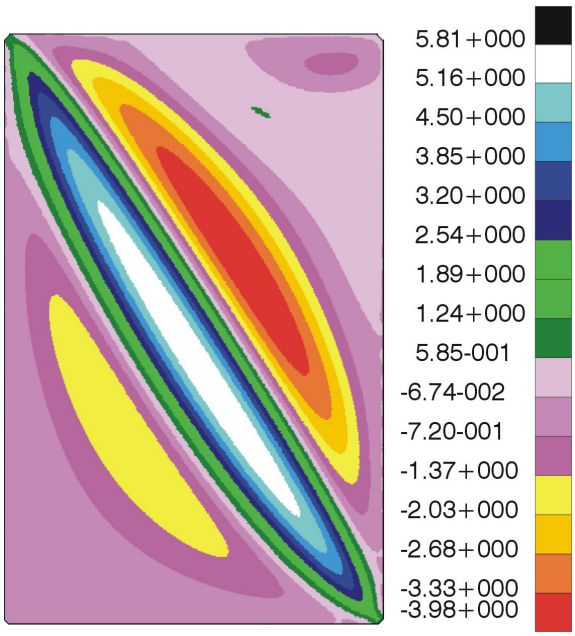


**Fig. 5**. Images of contour lines presenting the normal displacements: a) for the polycarbonate element, b) for the duralumin element

results obtained during experimental testing, both in terms of quality and quantity. However, none of the cases featured additional ridges in the corners. These types of discrepancies result from the idealised nature of the numerical model.

The second criterion of evaluating the numerical model was the compliance of the representative equilibrium paths demonstrating the deformation angle in the load function (Fig. 6).

The comparison of the representative balance paths, in both cases, shows high conformity between the experimental testing and the numerical calculations. The difference between the result of the numerical analysis and the experimental testing for the polycarbonate model does not exceed 9%. In the case of the aluminium alloy model, the discrepancy amounted to approx. 15%. In both cases, the numerical models demonstrated a slightly higher rigidity than real structures.

On the basis of the satisfactory compliance of the deformation form and the balance paths, it is possible to deem the stress distribution obtained as result of non-linear numerical analyses as reliable. The distribution of stress reduced acc. to the Huber-Misses-Hencky hypothesis is presented in Figure 7.

The analysis of the stress field distribution demonstrates a certain similarity between both analysed elements despite substantial differences in the deformation form. In both cases, maximum stress values and very high gradients can be observed in the corners of elements. Additionally, the diagonal features increased stress values in both cases, which is caused by the occurrence of strong bending effects along the ridges.

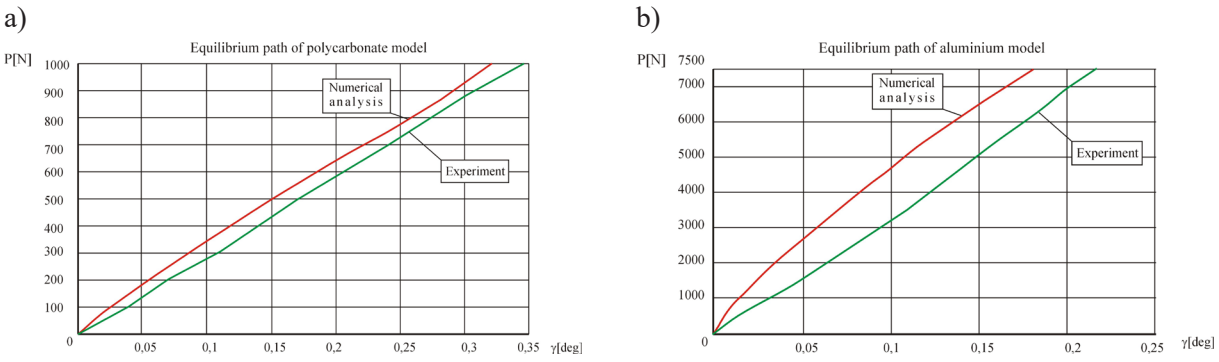


**Fig. 6**. Representative balance paths: a) for the polycarbonate element, b) for the duralumin element

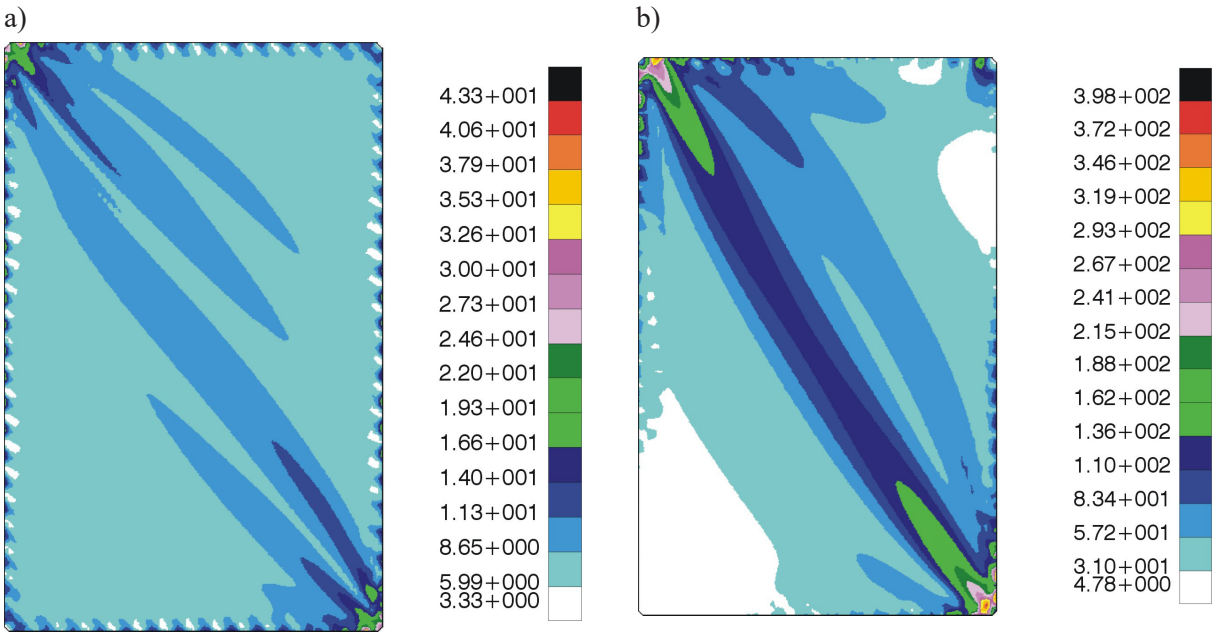


**Fig. 7**. Distribution of stress reduced acc. to the Huber-Misses-Henchy hypothesis: a) for the polycarbonate element, b) for the duralumin element

## CALCULATIONS AND FATIGUE TESTING

The stress distribution obtained using the non-linear numerical analyses became the basis for determining the fatigue strength of the analysed structures. The simulation for the aluminium alloy element was conducted using the MSC. Fatigue software [15]. Unfortunately, the program cannot be used for calculations of plastics, thereby limiting the ability of generating material models made solely of metal. The calculations were conducted on the basis of assumptions of the ε-n analysis (low-cycle fatigue) [10], indicating the areas exposed to 2 mm cracks. The calculations required generating a model made of the 2024 aluminium alloy [2,9] using the "Material Management" module. The alloy properties are presented in Table 1.

The calculations were conducted for sinusoidally variable cyclic loads with a symmetric nature. The conducted simulations allowed for obtaining a contour line image presenting the area exposed to fatigue cracks (Fig. 8).

The calculations demonstrated the occurrence of a 2 mm crack in the corner after approx. 24,900 cycles. Due to the high number of factors affecting the fatigue strength under actual conditions, experimental testing of fatigue was conducted for both polycarbonate and aluminium alloy structures. As result of the experimental testing, the polycarbonate model featured a field of over a dozen cracks of approx. 2 mm in length, located in the corner, after approx. 24,000 cycles. In the case of the aluminium alloy model, approx. 3 mm cracks were also observed in the corner after approx. 21,000 cycles. The fatigue damage is presented in Figure 9.

Further testing, conducted up to 35,000 cycles, cause a rapid expansion of the cracks in both cases and caused destruction in the mounting areas of the tested structure to the rigid frameworks. The form of destruction of the tested elements is presented in Figure 10.

In both cases, the form of destruction, obtained after 35,000 cycles, demonstrates certain qualitative similarities. This is especially visible

**Table 1.** Properties of alloy 2024

| UTS | YS | E | $\sigma_f'$ | B | c | $\varepsilon_f'$ | n' | K' |
|---|---|---|---|---|---|---|---|---|
| [MPa] | [MPa] | [MPa] | [MPa] | [-] | [-] | [-] | [-] | [MPa] |
| 470 | 372 | $0{,}74 \cdot 10^5$ | 1013.53 | -0.11 | -0.52 | 0.21 | 0.09 | 786 |

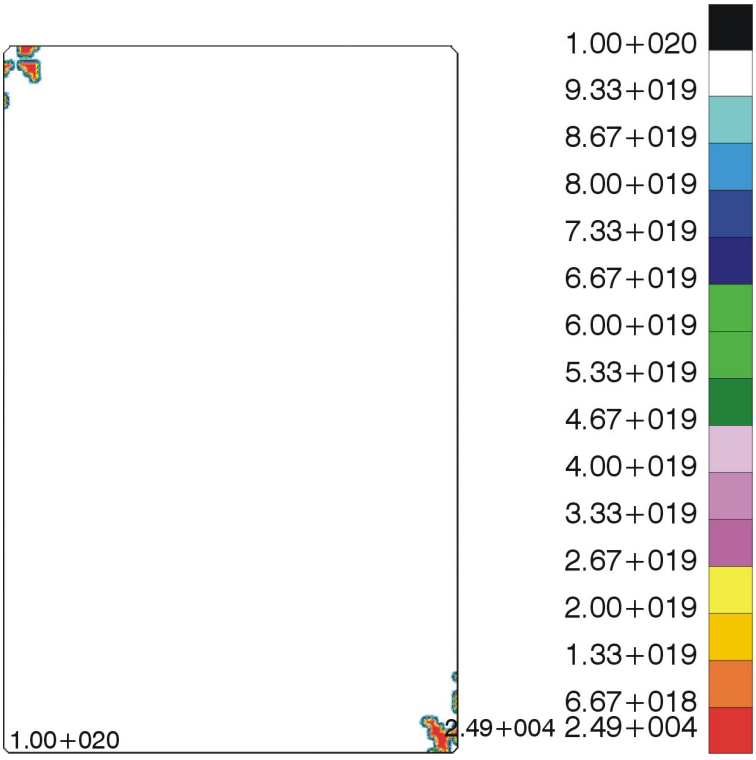


**Fig. 8**. Areas exposed to the occurrence of fatigue cracks

a) b)

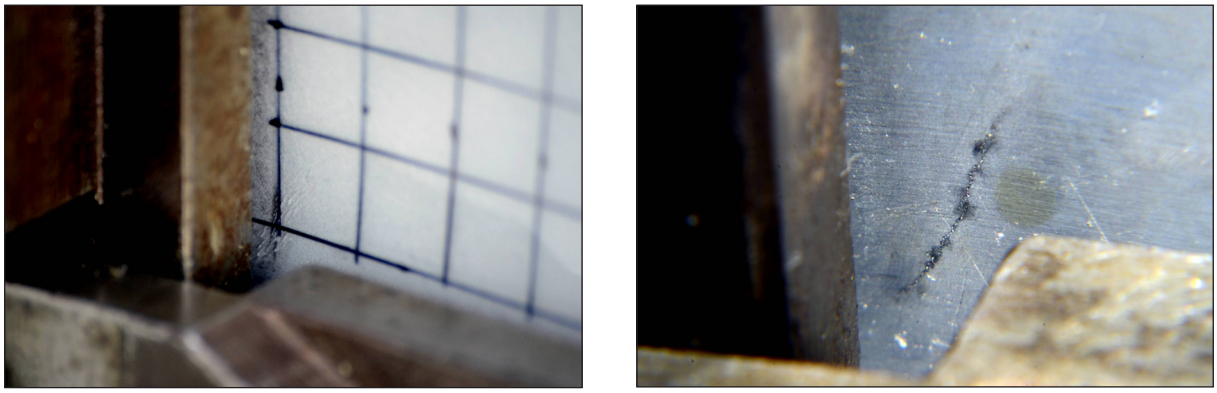

**Fig. 9**. Fatigue openings formed as result of cyclic loading: a) for the polycarbonate element, b) for the duralumin element

a) b)

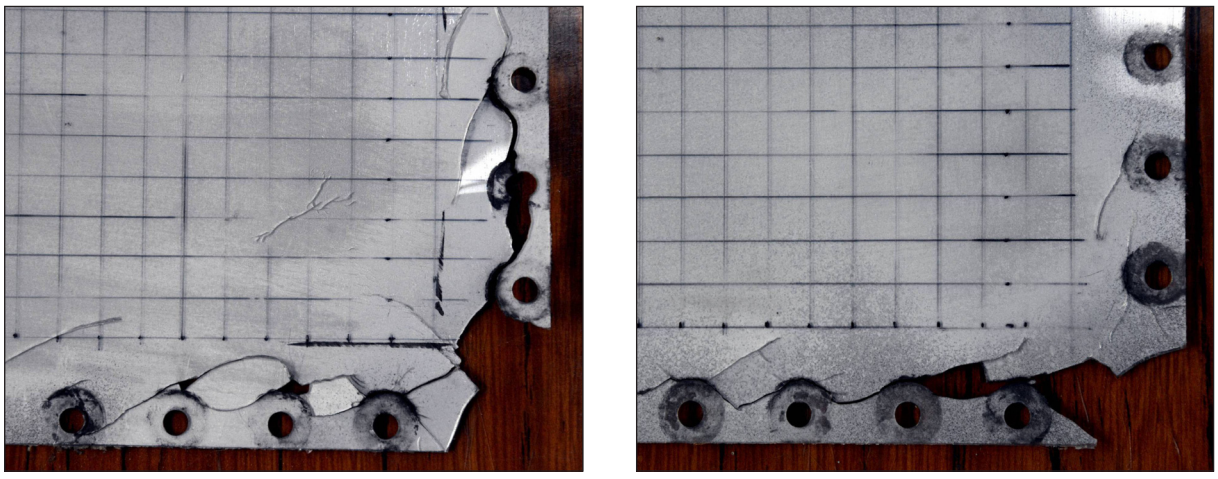

c) d)

**Fig. 10**. Fatigue cracks after 35,000 cycles: a) bottom left corner of the polycarbonate element, b) top right corner of the polycarbonate element, c) bottom left corner of the duralumin element, d) top right corner of the duralumin element

in relation to the corresponding areas presented in Figure 10b and 10d. Practically identical crack shapes are visible for elements made of various materials. In the case of the opposite corner in which the first crack appeared (Fig. 10a and 10c), it is possible to notice a similar crack along the element diagonal, as well as fatigue destruction of areas interoperating with mounting elements.

## CONCLUSIONS

The conducted numerical calculations and static experimental testing demonstrated the occurrence of various post-critical deformations, depending on the used material. The polycarbonate structure featured two dominant ridges, whereas the aluminium alloy structure featured a single ridge along the diagonal. These types of differences between the post-critical deformation forms obtained from elements made from various materials raise the question about the purposefulness of conducting this type of testing with the use of polymer model materials.

Despite substantial differences in the forms of deformation, the stress distribution obtained during numerical calculations demonstrated a certain similarity in the case of both materials used. The maximum stress values and their substantial concentration were observed in the plate corners, which suggests the risk of occurrence of fatigue cracks in these areas. The numerical simulations of fatigue performance conducted for the duralumin structure allowed for determining the area featuring the risk of occurrence of a 2 mm fatigue cracks field. The number of cycles after which there is a risk of occurrence of fatigue risks amounts to 24,900. The experimental testing with the use of oscillatory cyclic loads demonstrated the occurrence of fatigue damage after approx. 24,000 cycles in the case of the polycarbonate model and after approx. 21,000 cycles in the case of the aluminium alloy model. This provides a discrepancy in the results of 3.6% for the polycarbonate and 15.6% for the aluminium alloy. Due to the number of factors affecting the fatigue performance under actual conditions, the correspondence of the obtained results can be deemed as satisfactory.

## REFERENCES


1. Bathe K.J.: Finite element procedures in engineering analysis, Prentice-Hall, Englewood Cliffs 1982
2. Benachour N., Hadjoui A., Benachour M., Benguediab M.: Stress ratio and notch effect on fatigue crack initiation and propagation in 2024 Al-alloy. International Journal of Mechanical and Mechatronics Engineering, 5(7), 2011, 1384–1387.
3. Debski H.: Stability problems of compressed thin-walled structures. Advances in Science and Technology Research Journal, 12(4), 2018, 190–198.
4. Debski H., Teter A.: Numerical and experimental studies on the limit state of fibre-reinforced composite columns with a lipped channel section under quasi-static compression. Composite Structures, 133, 2015, 1–7.
5. Falkowicz K., Debski H.: Postbuckling behaviour of laminated plates with a cut-out. Advances in Science and Technology Research Journal, 11(1), 2017, 186–193.
6. Falkowicz K., Ferdynus M., Debski H.: Numerical analysis of compressed plates with a cut-out operating in the geometrically nonlinear range. Eksploatacja i Niezawodnosc – Maintenance and Reliability, 17(2), 2015, 222–227.
7. Felippa C.A.: Advanced finite element methods, (ASEN 5367) Dept. of Aerospace Eng. Sci. Bouilder, Colorado 2006.
8. Felippa C.A.: Nonlinear finite element methods, (ASEN 5107) Dept. of Aerospace Eng. Sci. Bouilder, Colorado 2006.
9. Khan S.S.: Low cycle lifetime assessment of Al 2024 alloys, Helmholtz-Zentrum Geesthacht, Zentrum für Material- und Küstenforschung GmbH, Geesthacht 2012.
10. Kocańda S., Szala J.: Podstawy obliczeń zmęczeniowych. Wydawnictwo Naukowe PWN, Warszawa 1997.
11. Kopecki T.: Numerical-experimental analysis of the post-buckling state of a multi-segment and multi-member thin-walled structure subjected to torsion; Journal of Theoretical and Applied Mechanics, 49(1), 2011, 227–242.
12. Kopecki T.: Numerical and experimental analysis of post-critical deformation states in a tensioned plate weakened by a crack. Journal of Theoretical and Applied Mechanics, 48(1), 2010, 45–70.
13. Kopecki T., Mazurek P.: Determination of stress distribution patterns in post-criticaldeformation states of thin-walled skins subjected to operating loads. Eksploatacja i Niezawodnosc – Maintenance and Reliability, 16(4), 2014, 608–615.
14. Kopecki T.; Święch Ł.: Experimental and numerical analysis of post-buckling deformation states of integrally stiffened thin-walled components of load-bearing aircraft structures. Journal of Theoretical and Applied Mechanics, 52(4), 2014, 905–915.
15. MSC Software: MSC Fatigue 2017, User's Guide. MSC Software Corporation, 2016.
16. MSC Software: MSC MARC 2017, User's Guide. MSC Software Corporation, 2016.
17. Wysmulski P., Debski H., Rozylo P., Falkowicz K.: A study of stability and post-critical behaviour of thin-walled composite profiles under compression; Eksploatacja i Niezawodnosc – Maintenance and Reliability, 18(4), 2016, 632–637.